

Spatial-spectral Terahertz Networks

Zheng Lin, Lifeng Wang, Bo Tan, and Xiang Li

Abstract

This paper focuses on the spatial-spectral terahertz (THz) networks, where transmitters equipped with the leaky-wave antennas send information to their receivers at the THz frequency bands. As a directional and nearly planar antenna, leaky-wave antenna allows for information transmissions with narrow beams and high antenna gains. The conventional large antenna arrays are confronted with challenging issues such as scaling limits and path discovery in the THz frequencies. Therefore, this work exploits the potential of leaky-wave antennas in the dense THz networks, to establish low-complexity THz links. By addressing the propagation angle-frequency coupling effects, the transmission rate is analyzed. The results show that leaky-wave antenna is efficient for achieving high-speed transmission rate and the co-channel interference management is not necessary when the THz transmitters with large subchannel bandwidths are not extremely dense. A simple subchannel allocation solution is proposed, which enhances the transmission rate compared with the same number of subchannels with equal allocation of frequency band. After subchannel allocation, a low-complexity power allocation method is proposed to improve the energy efficiency.

Index Terms

Terahertz networks, leaky-wave antenna, subchannel allocation, energy efficiency.

Z. Lin, L. Wang, and X. Li are with the Department of Electrical Engineering, Fudan University, Shanghai, China (E-mail: {lifengwang, lix}@fudan.edu.cn).

B. Tan is with the Faculty of Information Technology and Communication Sciences, Tampere University, Finland (E-mail: bo.tan@tuni.fi).

I. INTRODUCTION

The emerging services such as edge computing, immersive communication and tactile internet consume large frequency bands, to support high-speed data transmissions. Millimeter wave (mmWave) frequency bands have been applied in 5G (currently 24-50 GHz [1]). However, with the increasing numbers of smart devices and autonomous vehicles in the Internet-of-Things, more bandwidths are always required to strengthen the ultra-reliable and low latency communications (URLLC). Since the terahertz (THz) frequency bands are abundant, THz transmission is viewed as a promising 6G technology for reaching unprecedentedly high data rate [2–4].

To counteract the severe path loss in the higher frequencies, large antenna arrays with beam-forming techniques are adopted in 5G and its evolution [5]. In light of sparse-scattering mmWave channel environments, hardware costs and power consumptions, analog beamforming or hybrid beamforming approaches are recommended in the mmWave systems [5, 6]. The implementations of antenna arrays in the THz communications are investigated in [7–11], where various beamforming/precoding designs are proposed. However, using conventional antenna arrays has encountered many challenging issues in the THz frequencies, e.g., array architecture for accommodating highly dense THz antennas has to be re-designed [3], new phase modulation technique is demanded for developing THz phase shifters [12, 13], and existing path discovery methods may be infeasible [14]. Hence, it is essential to appropriately choose the THz antennas without adding significant link budget and power consumptions [4, 8, 12].

Leaky-wave antenna enables the wave to travel along the guiding architecture, to intensify the radio energy in preferred directions [15–17]. As a low-cost and easy-to-manufacture traveling-wave antenna, leaky-wave antenna can provide frequency-dependent narrow beams with high antenna gains [17], and own frequency-scanning capability [18, 19]. It has been utilized in many areas such as frequency-division multiplexing THz communication [20], THz radar sensing [21–23], link discovery [14], and physical layer security enhancement [24]. One key feature of the leaky-wave antenna is that it enables the information transmissions in a spatial-spectral manner, i.e., frequencies are correlated with the transmission directions. There are also other directional antenna designs such as horn and lens antennas. In particular, horn antenna has been used in the mmWave and THz channel measurements [3, 25] and fixed wireless access for THz communication systems [2]. Unlike leaky-wave antenna, these antennas are inherently fixed beam solutions with a single direction and how to integrate them for expanding coverage needs to be

properly addressed [4].

The aforementioned works only study the case of point-to-point THz communication with leaky-wave antenna [20, 24]. When there exist large numbers of transceivers in the THz networks with massive connections, the co-channel interference has an adverse effect on the transmission rate, which needs to be evaluated. Moreover, THz transmissions utilize much larger frequency bands, and subchannel allocation plays a crucial role in controlling the number of subchannels while guaranteeing the targeted transmission rate, such that the peak-to-average power ratio (PAPR) can be kept in a low level. Unfortunately, few research contributions investigate the subchannel allocation when implementing the leaky-wave antenna in the THz communications. In addition, energy efficiency enhancement is of importance, in order to reduce the power consumptions. Therefore, we adopt the leaky-wave antennas to harness the THz waves in the dense THz networks, and the main contributions are concluded as follows:

- **THz Networks with Leaky-wave Antennas:** In the considered THz networks, each transmitter equipped with a leaky-wave antenna (TE_1 mode) sends information to its corresponding receiver with an omnidirectional antenna. Since the effects of the none-line-of-sight (NLoS) links is negligible in the THz frequencies, we focus on the dominant line-of-sight (LoS) links. As a useful tool to evaluate the performance behavior in the large-scale wireless networks [26], stochastic geometry is employed to model the spatial distributions of transmitters.
- **Average Transmission Rate and Subchannel Allocation:** In light of the spatial energy distribution under the leaky-wave antenna radiation, the average transmission rate is quantified for an arbitrary THz subchannel. Considering the fact that different THz frequencies have different sizes of subchannel bandwidths and undergo significantly different channel conditions, a closed-form solution for subchannel allocation is proposed to enhance the transmission rate with a small number of subchannels. Then, a low-complexity power allocation is designed to maximize the average energy efficiency (EE) over the number of subchannels.
- **Design Insights:** Our results show that high-speed transmission rate is achievable in the dense THz networks with leaky-wave antennas, and noise-limited phenomenon occurs when the transmitters with large subchannel bandwidths are not super dense. The average transmission rate can vary dramatically with slightly different values of aperture length or attenuation coefficient. The proposed subchannel allocation improves the average transmission rate in

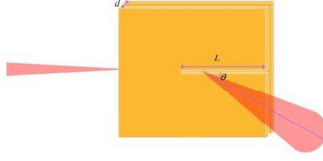


Fig. 1. An illustration of leaky-wave antenna with the lowest transverse-electric (TE_1) mode.

the leaky-wave antenna systems, compared with the same number of subchannels with equal allocation of frequency band. Our power allocation method can improve the EE. It is demonstrated that center frequencies with the maximum radiated energy may not be the best option when ignoring the channel gains, and slightly adding the attenuation coefficient could dramatically improve the average transmission rate for large frequency bandwidths, since more frequencies are in the main-lobe that captures large radiated energy.

The rest of this paper is organized as follows. The considered system model is described in Section II, and the average transmission rate is analyzed based on stochastic geometry in Section III. Subchannel allocation is determined in Section IV. Section V focuses on the EE enhancement. Section VI covers the simulation results. Finally, some concluding remarks and future work are presented in Section VII.

II. SYSTEM DESCRIPTIONS

As shown in Fig. 1, the guiding structure of a 1D leaky-wave antenna consists of a rectangular waveguide with a longitudinal slit, where d , L and θ denote the inter-plate distance, aperture length and propagation angle, respectively. In the large-scale THz networks, each transmitter equipped with a leaky-wave antenna communicates with its corresponding receiver equipped with an omnidirectional antenna (namely single-input single-output), and they are randomly located following a homogeneous Poisson point process (PPP) Φ_{THz} with density λ_{THz} .

Given a THz frequency f and the propagation angle θ ($0 < \theta < 90^\circ$), the far-field radiation pattern of the considered leaky-wave antenna is given by [27]

$$G(f, \theta) = L \text{sinc} \left[(-j\alpha - k_0 \cos \theta + \beta) \frac{L}{2} \right], \quad (1)$$

where $j = \sqrt{-1}$, α is the attenuation coefficient due to the power absorption in the structure, $k_0 = 2\pi f/c$ with the speed of light c is the wavenumber of the free-space, $\beta = k_0 \sqrt{1 - \left(\frac{f_{\text{co}}}{f}\right)^2}$

is the phase constant of the TE_1 mode based traveling wave, in which $f_{co} = \frac{c}{2d}$ is the cutoff frequency [28]. The frequencies should be larger than the cutoff frequency (i.e., $f > f_{co}$), to enable that THz wave propagates away from the antenna structure, namely fast wave radiation [27]. Given a LoS direction θ of a receiver, the maximum level of the radiation can be obtained by using the frequency as follows [17, 20]:

$$f^{\max}(\theta) = \frac{f_{co}}{\sin \theta}. \quad (2)$$

As shown in Fig. 2, the frequency for maximizing the radiation is reliant on the beam angle and lower attenuation coefficient results in narrower beam.

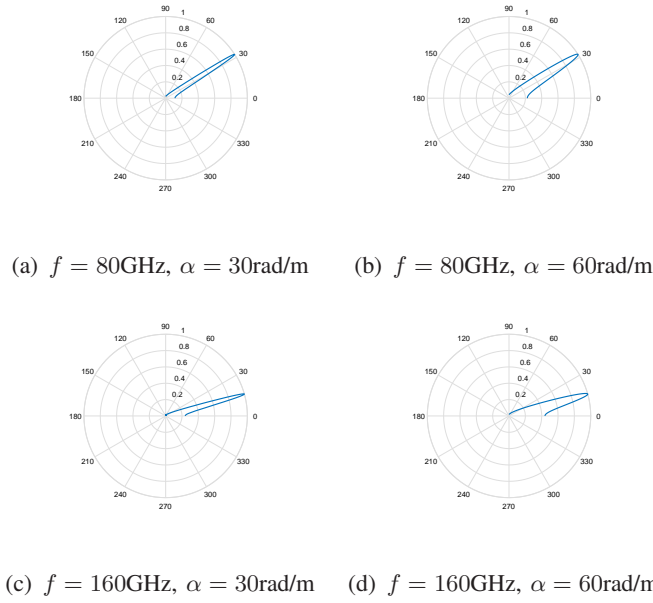


Fig. 2. Examples of the leaky-wave antenna's radiation pattern with $L = 5.5\text{cm}$ and $d = 3.5\text{mm}$.

Although transmitters may have different propagation angles and send their information with the maximum antenna gains in the different THz frequencies given by (2), co-channel interference still exists in the large-scale THz networks, where the nearby transceivers may use the same subchannels for the low propagation angle difference $\Delta\theta$. As measured in [20], for a given $\Delta\theta$, its closely related frequency bandwidth is

$$B(\theta) = \frac{f_{co}\Delta\theta}{\sin \theta \tan \theta}, \quad (3)$$

which can be interpreted as the range of the frequencies whose levels of radiation are close to that at $f^{\max}(\theta)$. In addition, different transmitters may have different cutoff frequencies

and propagation angles, but leverage the same frequency, as indicated in (2). Therefore, the transmission rate of a subchannel from the typical transmitter to its receiver (at the origin) can be expressed as

$$R_o = B_o \log_2 \left(1 + \frac{q_t \tilde{G}(f_o, \theta_o) \ell(r_o)}{\sum_{i \in \tilde{\Phi}_{\text{THz}/o}} q_t \tilde{G}(f_i, \varphi_i) \ell(r_i) + \sigma_o^2} \right), \quad (4)$$

where B_o is the subchannel bandwidth, q_t is the transmit power spectral density (PSD) of the typical transmitter, $\tilde{G}(f, \theta) = \xi G(f, \theta)$ with a constant ξ^1 is the effective antenna gain, θ_o is the typical propagation angle, $\ell(r)$ is the path loss function with the communication distance r , f_o and f_i are the frequencies used by the typical transmitter and the i -th interferer, respectively, φ_i is the interfering link direction from the i -th transmitter (interferer) to the typical receiver, which is assumed to be independently and uniformly distributed in $(0, \frac{\pi}{2})$, σ_o^2 is the PSD of the noise. Here, $\ell(r) = \rho(f) (\max(D, r))^{-\eta}$ with the intercept $\rho(f) = (\frac{c}{4\pi f})^2$, reference distance D and path loss exponent η [25, 29]. The small-scale fading effect is omitted since it is insignificant in LoS links with directional antennas in the higher frequencies [30]. It should be noted in (4) that the frequency f_i solely depends on the link between the i -th transmitter and its corresponding receiver.

III. AVERAGE TRANSMISSION RATE

In this section, we evaluate the average transmission rate in the dense THz networks with leaky-wave antennas, which is an important performance indicator. Like mmWave, THz communication is also susceptible to the blockage. There are empirical (e.g., 3GPP) and analytical (e.g., random shape theory) blockage models [29], hence we consider the generalized case, i.e., the LoS probability function for a THz link at a distance r is denoted as $P_{\text{LoS}}(r)$. The average transmission rate is calculated as [31, 32]

$$\begin{aligned} \overline{R}_o &= \mathbb{E}[R_o] \\ &= \frac{B_o}{\ln 2} \int_0^\infty \frac{1}{s} \left(1 - e^{-sY(\max(D, r_o))^{-\eta_{\text{LoS}}}} \right) \Theta(s) e^{-s\sigma_o^2} ds, \end{aligned} \quad (5)$$

where $\Theta(s) = \mathbb{E}[e^{-sI}]$, η_{LoS} is the LoS path loss exponent, $Y = q_t \tilde{G}(f_o, \theta_o) \rho$, and the interference $I = \sum_{i \in \tilde{\Phi}_{\text{THz}/o}} q_t \tilde{G}(f_i, \varphi_i) \ell(r_i)$. The frequency of the typical transmission link

¹Through measuring the effective antenna gain for a particular leaky-wave antenna structure, ξ can be easily obtained and known a priori.

is assumed to be $f_o = f^{\max}(\theta_o)$, i.e., main-lobe gain can be obtained at the typical receiver. It is obvious that co-channel interference occurs when the frequencies used by the interferers are in the range $[f_o - \frac{B_o}{2}, f_o + \frac{B_o}{2}]$. We consider the worst-case scenario that all the transmitters are homogeneous (namely identical cutoff frequency), thus the typical receiver is more likely to be covered by the main-lobes of the interferers' leaky-wave antennas. According to (3), the probability that a transmitter uses the frequency band B_o at f_o is given by

$$P_{f_o} = \int_0^{\Delta\theta_o} \frac{2}{\pi} d\theta = \frac{2B_o \sin \theta_o \tan \theta_o}{\pi f_{co}}. \quad (6)$$

Based on the thinning theorem [26], the density of the PPP $\tilde{\Phi}_{\text{THz}}$ is $\lambda_{\text{THz}} P_{f_o}$. Since the interference resulted from NLoS links is negligible in the THz frequencies, the LoS interferers can be modeled as the non-homogeneous PPP with the density function $\lambda_{\text{THz}} P_{f_o} P_{\text{LoS}}(r)$ [29]. Therefore, by using the Laplace functional of the PPP, $\Theta(s)$ can be evaluated as

$$\Theta(s) = \exp \left(-2\pi \lambda_{\text{THz}} P_{f_o} \int_0^\infty P_{\text{LoS}}(r) (1 - \Xi(r)) r dr \right), \quad (7)$$

where $\Xi(r)$ is

$$\Xi(r) = \mathbb{E} \left[e^{-sq_t \tilde{G}(f_o, \varphi_i) \rho(\max\{D, r\})^{-\eta_{\text{LoS}}}} \right]. \quad (8)$$

To solve (8), we first need to determine the directions of the interfering links in the spatial-domain, which have a detrimental effect on the transmission rate. It is seen from (3) that the interfering link direction φ_i meets the following condition:

$$\varphi_i \in \left[\theta_o - \frac{\Delta\theta_o}{2}, \theta_o + \frac{\Delta\theta_o}{2} \right], \quad (9)$$

where $\Delta\theta_o = \frac{B_o \sin \theta_o \tan \theta_o}{f_{co}}$. Based on (9), $\Xi(r)$ is explicitly given by

$$\Xi(r) = \int_{\theta_o - \Delta\theta_o/2}^{\theta_o + \Delta\theta_o/2} \frac{2}{\pi} e^{-sq_t \tilde{G}(f_o, \varphi) \rho(\max\{D, r\})^{-\eta_{\text{LoS}}}} d\varphi. \quad (10)$$

Substituting (7) and (10) into (5), we can obtain the average transmission rate given by (11).

Considering the fact that $G(f_o, \varphi) \leq G(f_o, \theta_o)$ as $\varphi \in [\theta_o - \frac{\Delta\theta_o}{2}, \theta_o + \frac{\Delta\theta_o}{2}]$, the lower bound of the average transmission rate is

$$\begin{aligned} \overline{R}_o^L = & \frac{B_o}{\ln 2} \int_0^\infty \frac{1}{s} \left(1 - e^{-sY(\max(D, r_o))^{-\eta_{\text{LoS}}}} \right) e^{-s\sigma_o^2} \exp \left[-2\pi \lambda_{\text{THz}} P_{f_o} \int_0^\infty P_{\text{LoS}}(r) \left(1 - \frac{2\Delta\theta_o}{\pi} \right. \right. \\ & \left. \left. \times e^{-sY(\max\{D, r\})^{-\eta_{\text{LoS}}}} \right) r dr \right] ds. \end{aligned} \quad (12)$$

$$\bar{R}_o = \frac{B_o}{\ln 2} \int_0^\infty \frac{1}{s} \left(1 - e^{-sY(\max(D, r_o))^{-\eta_{\text{LoS}}}} \right) \exp \left(-s\sigma_o^2 - 2\pi\lambda_{\text{THz}}P_{f_o} \int_0^\infty P_{\text{LoS}}(r) (1 - \Xi(r)) r dr \right) ds \quad (11)$$

with $\Xi(r)$ given by (10).

The average transmission rate given by (5) is derived for an arbitrary subchannel. In practice, it is essential to properly determine the number of subchannels and each subchannel bandwidth for a large number of THz bandwidths. In the next section, we provide an efficient subchannel allocation solution.

IV. SUBCHANNEL ALLOCATION

In the THz systems, the abundance of bandwidths need to be divided into many subchannels, and the bandwidth of each subchannel depends on the effective antenna gain of the leaky-wave antenna and the channel condition. However, multi-carrier transmissions result in PAPR issue and adding subchannels could create higher PAPR [33, 34]. The use of large mmWave bandwidths with high PAPR waveforms has already posed demanding power amplifier requirements in 5G systems [35, 36]. Therefore, one of our aims is to determine the minimum number of subchannels for maximizing the transmission rate given the THz bandwidths, which is helpful to tune the number of subchannels for PAPR reduction. Moreover, the center frequency of each subchannel has to be appropriately selected, and the frequency given by (2) for obtaining the maximum radiation energy may not be the best option, since different THz frequencies have varying THz channel gains with significant path loss [3]. In addition, not all of available THz bandwidths could be applied under the quality of service (QoS) constraint when using the leaky-wave antenna.

As mentioned above, the considered subchannel allocation problem is formulated as

$$\begin{aligned} & \max_{\mathbf{B}, \mathbf{f}} \sum_n B_n \log_2 \left(1 + \frac{\gamma_n(f_n)}{\sigma_o^2} \right) \\ & \text{s.t. C1 : } \sum_n B_n \leq B_{\text{total}}, \\ & \text{C2 : } \bigcap_n \left\{ f \mid f \in \left[f_n - \frac{B_n}{2}, f_n + \frac{B_n}{2} \right] \right\} = \emptyset, \end{aligned} \quad (13)$$

$$\begin{aligned}
\text{C3} : & \frac{\gamma_n(f_n)}{\sigma_o^2} \geq \gamma_{\text{th}}, \quad \forall n, \\
\text{C4} : & \left\| \gamma_n \left(f_n - \frac{B_n}{2} \right)_{\text{dB}} - \gamma_n \left(f_n + \frac{B_n}{2} \right)_{\text{dB}} \right\| \leq \varepsilon, \quad \forall n, \\
\text{C5} : & B_n \geq 0, \quad \forall n,
\end{aligned}$$

where $\mathbf{B} = [B_n]$, $\mathbf{f} = [f_n]$, and $\gamma_n(f_n) = q_t \tilde{G}(f_n, \theta) \ell(r)$ is the receive PSD. Constraint C1 describes the total available bandwidth B_{total} ; C2 ensures that there is no overlap between subchannels; C3 is the QoS constraint with the threshold γ_{th} ; C4 ensures that the received signal power (signal strength) difference is below a small value ε in the frequencies of a subchannel; C4 ensures that B_n is non-negative value. In problem (13), interference is negligible because of noise-limited THz networks, as confirmed in Section VI.

Since the antenna gain cannot be explicitly calculated, solving the combinatorial problem (13) is more challenging. Thus, we provide a low-complexity approach to deal with it. One feature of using leaky-wave antenna is that large range of THz frequencies (above 0.1 THz) have nearly identical level of radiation and similar signal strength along a propagation angle, as seen in Fig. 3 (Similar result also seen in Fig. 10 of [14]). Moreover, the recent THz channel modeling works [37, 38] have demonstrated that given the communication distance within 100m, pure free-space path loss (FSPL) model can well predict the channel of LoS THz link for the 0.1-0.45 THz frequency band, which is the potential 6G frequency band [3]. Therefore, based on FSPL model, constraint C4 in (13) can be rewritten as

$$B_n \leq 2f_n \frac{10^{\varepsilon/20} - 1}{10^{\varepsilon/20} + 1}. \quad (14)$$

We note that different values of the attenuation coefficient α primarily influence the main-lobe and its nearby side-lobe levels, and have little effect on their trend in the frequency range of interest [16], which is also shown in [27]. Thus we can approximate problem (13) by letting $\alpha = 0$. In addition, frequencies of interest need to be close to $f^{\text{max}}(\theta)$ given by (2), in order to obtain large radiated energy. As such, by applying the Taylor series expansion truncated to the first order at $f^{\text{max}}(\theta)$, $G(f, \theta)$ with $\alpha = 0$ in the frequency range of interest can be evaluated as

$$G(f, \theta) \approx L - \frac{L^3}{24} (\beta - k_0 \cos \theta)^2. \quad (15)$$

By considering (14), (15) and $\beta \approx k_0 \left(1 - \frac{f_{\text{co}}^2}{2f^2} \right)$, problem (13) is rewritten as

$$\max_{\mathbf{B}, \mathbf{f}} \sum_n B_n \log_2 (1 + F_{\text{SNR}}(f_n)) \quad (16)$$

s.t. C1, C2, C5,

$$\tilde{C}3 : F_{\text{SNR}}(f_n) \geq \gamma_{\text{th}}, \quad \forall n,$$

$$\tilde{C}4 : (14), \quad \forall n,$$

where $F_{\text{SNR}}(f_n) = \frac{q_t \ell(r)}{\sigma_o^2} \left(L - \frac{L^3 k_o^2}{24} \left(1 - \frac{f_{co}^2}{2f_n^2} - \cos \theta \right)^2 \right)$. To deal with the combinatorial constraint C2, we propose a greedy-based solution. We first find the best f_1^* by solving the following subproblem

$$\begin{aligned} & \max_{f_1} F_{\text{SNR}}(f_1) \\ & \text{s.t. } \tilde{C}3, \end{aligned} \tag{17}$$

which means the best center frequency that has the largest signal strength is first chosen. Based on (17), we have

Theorem 1: The optimal solution of the subproblem (17) is given by

$$f_1^* = \mathbf{1} \left(F_{\text{SNR}}(f_1^{(1)}) \geq \gamma_{\text{th}} \right) f_1^{(1)}, \tag{18}$$

where $f_1^{(1)} = \frac{f_{co}^2}{\sqrt{\frac{12c^2}{L^2\pi^2} + 2(1-\cos \theta_o)f_{co}^2}}$, and $\mathbf{1}(A)$ represents the indicator function that returns one if the condition A is met.

Proof 1: See Appendix A.

It is shown from **Theorem 1** that while the center frequency given by (2) has the maximum radiated energy, it may not necessarily achieve the largest signal strength without considering the channel environments. Based on **Theorem 1** and problem (16), the optimal bandwidth of the first subchannel with the center frequency f_1^* is $B_1^* = 2f_1^* \frac{10^{\varepsilon/20} - 1}{10^{\varepsilon/20} + 1}$. As such, we can obtain the center frequency of the n -th subchannel and the corresponding the subchannel bandwidth as follows:

Theorem 2: The optimal center frequency of the n -th ($n \geq 2$) subchannel is given by

$$f_n^* = \mathbf{1} (F_{\text{SNR}}(f_n) \geq \gamma_{\text{th}}) f_n, \tag{19}$$

where

$$f_n = \begin{cases} \Lambda^{-1} f_{\min}, & \text{if } \hat{F}(\Lambda^{-1} f_{\min}) > \hat{F}(\Lambda f_{\max}), \\ \Lambda f_{\max}, & \text{otherwise,} \end{cases} \tag{20}$$

with $\Lambda = 10^{\varepsilon/20}$, $f_{\min} = \min \{f_1^*, \dots, f_{n-1}^*\}$, $f_{\max} = \max \{f_1^*, \dots, f_{n-1}^*\}$, and $\hat{F}(f) = f^{-2} \left(L - \frac{L^3 \pi^2 f^2}{6c^2} \left(1 - \frac{f_{co}^2}{2f^2} - \cos \theta \right)^2 \right)$. The corresponding subchannel bandwidth is

$$B_n^* = \min \left\{ 2f_n^* \frac{10^{\varepsilon/20} - 1}{10^{\varepsilon/20} + 1}, B_{total} - \sum_{b=1}^{n-1} B_b \right\}, \quad (21)$$

respectively.

Proof 2: See Appendix B.

Based on **Theorem 1** and **Theorem 2**, we obtain a low-complexity solution of problem (13), which is concluded in **Algorithm 1**.

Algorithm 1 Solution of Problem (13)

- 1: Initialize the number of subchannels $n = 1$.
- 2: **if** $n = 1$, **then**
- 3: Calculate the center frequency f_1^* and bandwidth $B_1^* = 2f_1^* \frac{10^{\varepsilon/20} - 1}{10^{\varepsilon/20} + 1}$ of the first subchannel based on **Theorem 1**.
- 4: **else**
- 5: **Repeat**
- 6: $n = n + 1$.
- 7: Calculate the center frequency f_n^* and bandwidth B_n^* of the n -th subchannel based on **Theorem 2**.
- 8: **Until** $B_n^* = 0$.
- 9: $N \leftarrow n - 1$.
- 10: **end if**

Output: Subchannel allocation $(f_n^*, B_n^*), n = 1, \dots, N$.

V. ENERGY EFFICIENCY ENHANCEMENT

The prior section has shown that the number of subchannels N and the bandwidth of each subchannel can be easily determined with the help of **Algorithm 1**. To reduce the power consumption in the THz system with leaky-wave antenna, we seek to maximize the average EE with respect to the transmit PSDs $\{q_n\}$ of the subchannels. Based on Sections II-IV, the considered problem is formulated as

$$\max_{\mathbf{q}} \frac{1}{N} \sum_{n=1}^N \frac{\log_2(1 + q_n \Xi_n)}{q_n + q_c} \quad (22)$$

$$\text{s.t. } \hat{\text{C}}1 : 0 < q_n \leq q_{\max}, \quad \forall n,$$

$$\hat{\text{C}}2 : q_n \Xi_n \geq \gamma_{\text{th}}, \quad \forall n,$$

where $\mathbf{q} = [q_n]$, $\Xi_n = \frac{\tilde{G}(f_n, \theta) \ell(r)}{\sigma_o^2}$, and q_c is the PSD due to the hardware's power consumptions. Constraint $\hat{\text{C}}1$ is the transmit PSD's feasible range with the maximum value q_{\max} , and $\hat{\text{C}}2$ is the QoS constraint. Problem (22) can be decomposed into N subproblems:

$$\begin{aligned} & \max_{q_n} \frac{\log_2(1 + q_n \Xi_n)}{q_n + q_c} \\ & \text{s.t. } \hat{\text{C}}1, \quad \hat{\text{C}}2. \end{aligned} \quad (23)$$

Then, we have the following theorem:

Theorem 3: The optimal transmit PSD of the n -th subchannel is given by

$$q_n^* = \begin{cases} q_{\max}, & \text{if } \hat{F}_{\text{EE}}(q_{\max}) \geq 0, \\ \max\left\{q_o, \frac{\gamma_{\text{th}}}{\Xi_n}\right\}, & \text{otherwise,} \end{cases} \quad (24)$$

where $\hat{F}_{\text{EE}}(q) = \frac{q+q_c}{1+q\Xi_n} \Xi_n - \ln(1 + q\Xi_n)$, and q_o with $\hat{F}_{\text{EE}}(q_o) = 0$ can be easily obtained by using a one-dimension search in $q_o \in (0, q_{\max}]$ since $\hat{F}_{\text{EE}}(q)$ is a decreasing function.

Proof 3: See Appendix C.

Thus, we obtain a closed-form power allocation solution for enhancing the EE.

VI. SIMULATION RESULTS

This section provides numerical results to validate our analysis and the efficiency of the proposed solutions for subchannel allocation and EE enhancement. In the simulations, the transmit PSD is $q_t = -71.76\text{dBm/Hz}$, the noise's PSD is $\sigma_o^2 = -168\text{dBm/Hz}$, the inter-plate distance is $d = 3.5\text{mm}$, $\xi = 1$, the free-space path loss model is applied with the LoS path loss exponent $\eta_{\text{LoS}} = 2$ [37, 38], and the reference distance $D = 1$. Based on the 3GPP blockage model [39], the LoS probability function $P_{\text{LoS}}(r)$ with a distance r is given by

$$P_{\text{LoS}}(r) = e^{-r/a_1} + (1 - e^{-r/a_1}) \min\left(\frac{a_2}{r}, 1\right), \quad (25)$$

where $a_1 = 63\text{m}$ and $a_2 = 18\text{m}$. The other simulation parameters are detailed in the following simulation results.

A. Average Transmission Rate Analysis

In this subsection, we analyze the effects of different system parameters on the average transmission rate. The analytical results for average transmission rate are obtained from (11).

Fig. 4 shows that our analysis has a good match with the Monte Carlo simulations for different values of communication distance and attenuation coefficient, and using leaky-wave antenna enables the THz networks to be noise-limited in the presence of highly dense transmitters. In the THz frequencies, slightly increasing the communication distance between a typical transmitter and its receiver can significantly reduce the average transmission rate, due to the higher path loss. In addition, different attenuation coefficients have negligible effect on the level of interference.

Fig. 5 shows that THz networks with leaky-wave antennas become interference-limited only when extremely dense transmitters (e.g., $\lambda_{\text{THz}} = 10^0/\text{m}^2$ in this figure) utilize large subchannel bandwidth. Moreover, we see that increasing the subchannel bandwidth results in higher level of interference as $\lambda_{\text{THz}} > 10^{-1}/\text{m}^2$. The reason is that large subchannel bandwidth corresponds to higher propagation angle difference $\Delta\theta_o$ (See (3)), the effects of which are two-fold: 1) More interferers use the same frequency band; 2) The typical receiver is covered by more interferers.

Fig. 6 shows that the average transmission rate significantly decreases when using higher THz frequency bands. Again, we see that the analytical results have an agreement with the Monte Carlo simulations for different values of THz frequency and aperture length. For higher THz frequencies (e.g., above 300GHz in this figure), the effect of aperture length on the interference is marginal.

B. Subchannel Allocation

In this subsection, we focus on the efficiency of the proposed subchannel allocation solution through comparison with the same number of subchannels with equal allocation of frequency band. In the simulations, the propagation angle from the transmitter to the receiver is uniformly distributed, i.e., $\theta \in U(0, \frac{\pi}{2})$, the communication distance is uniformly distributed within the coverage radius r_{max} , the aperture length $L = 0.06\text{m}$, $\gamma_{\text{th}} = -6.5\text{dB}$ [40], $\varepsilon = 0.2\text{dB}$, the continuous broadband spectrum ranging from 100 GHz to 350 GHz is considered, namely $f \in [100, 350](\text{GHz})$, and the number of trials is 3×10^4 . The proposed solution is provided based on **Algorithm 1**, which is in comparison with the equal allocation method (namely equal allocation of frequency band with the same number of subchannels and center frequency given by (2)).

Fig. 7 shows that the proposed solution outperforms the equal allocation method for different total bandwidths. Slightly increasing the α value can improve the average transmission rate when adding the frequency bandwidths. The reason is that based on [16, eq. (7.25)], increasing the α value creates larger beamwidth, which means more frequencies are in the main-lobe that captures large radiated energy, as indicated in (3) and Fig 3. It is seen from Fig. 7(b) that the proposed solution can well control the number of subchannels, e.g., in this figure, the number of subchannels increases by about 60% when doubling the total bandwidth. There exist more subchannels for larger α and total bandwidth, due to the fact that more frequencies in the main-lobe satisfy the QoS constraint and can be applied.

Fig. 8 shows that the proposed solution achieves better performance than equal allocation method for different coverage areas. When the coverage area of the transmitter is expanded, the performance difference between the far-away receiver and the nearby one is significant, due to the higher path loss in the THz frequencies. An interesting phenomenon is seen in Fig. 8(b), i.e., the average number of subchannels decreases for larger coverage radius and lower attenuation coefficient. The reason is that lower attenuation coefficient value creates narrower beamwidth, and thus more frequencies are in the side-lobes (lower signal strength), which means that more frequencies cannot meet the QoS constraint.

Fig. 9 shows that the proposed solution achieves better performance than equal allocation method for different aperture lengths. We see that slightly changing the aperture length can have a big impact on the average transmission rate. Such impact is more significant when increasing the α value. It is indicated from Fig. 9(b) that slightly changing the aperture length also has a big impact on the number of subchannels.

C. Energy Efficiency

In this subsection, numerical results are presented by using **Theorem 3**, and the efficiency of the proposed power allocation solution is confirmed in comparison with the equal power allocation (namely $q_n = q_{\max}$, $n = 1, \dots, N$). In the simulations, $q_{\max} = -71.76\text{dBm/Hz}$, $q_c = -81.76\text{dBm/Hz}$, the communication distance is uniformly distributed within the coverage radius $r_{\max} = 100\text{m}$ and other basic simulation parameters are set as mentioned in subsection VI-B.

Fig. 10(a) shows that the proposed solution achieves better EE than equal power allocation method for different total bandwidths, and the advantage of the proposed solution is more significant when increasing the total bandwidths or α value. The reason is that the increase of the

total bandwidth or α value enables more available subchannels (See Fig. 7), and the proposed solution can reduce more power consumptions. Fig. 10(b) shows that the proposed solution performs better than equal power allocation method for different attenuation coefficients. As mentioned before, the proposed solution saves more energy when increasing the α value. We see that slightly changing the aperture length also has a big impact on the EE.

VII. CONCLUSIONS AND FUTURE WORK

This paper concentrated on the benefits of using leaky-wave antenna in the THz networks, where each transmitter leveraged a single leaky-wave antenna to create high antenna gain. We first derived the average transmission rate in the dense THz networks, which demonstrated the noise-limited behavior of using leaky-wave antenna. Our results showed that the effect of interference becomes significant only when the subchannel bandwidth is large enough and the transmitters are extremely dense. Then, we addressed the subchannel allocation issue for large THz frequency bands, which is crucial for meeting the QoS constraint and tackling the PAPR problem. In light of leaky-wave antenna's characteristics, a closed-form solution for subchannel allocation was developed. The results confirmed the efficiency of the proposed subchannel allocation solution in comparison with the equal allocation method, which indicated that the attenuation coefficient of the leaky-wave antenna has a big effect on the subchannel allocation. Furthermore, we developed a low-complexity power allocation method for EE enhancement, and the results confirmed that the proposed method achieved better EE performance than the equal power allocation.

While this work has shown the opportunities of leaky-wave antenna in the large-scale THz networks, more research efforts are required to further evaluate the performance behaviors from different perspectives and develop various transmission designs with leaky-wave antennas. In particular, the spatial-spectral feature of leaky-wave antenna means that the value of the attenuation coefficient has to be properly designed. The reason is that larger attenuation coefficient values allow more frequencies to be in the main-lobe, which could improve the transmission rate, however, it also brings in more interference for the ultra-dense THz networks. Another area that warrants further research is the transmission design in the case of each transmitter with multiple leaky-wave antennas. In this case, multiplexing gains are more likely to be achieved in the frequency-domain but it may need to be delicately designed for achieving large array gains due to the leaky-wave antenna's spatial-spectral feature, which is quite different from the beamforming/precoding designs with conventional large arrays in the sub-6 GHz and

mmWave frequencies. In addition, further studies are needed for the scenarios such as multi-user transmissions, multi-tier transmissions with sub-6 GHz, mmWave and THz tiers, cognitive radio, wiretap channels, integrated access and backhaul etc.

APPENDIX A: PROOF OF THEOREM 1

Since $\ell(r_o) = (\frac{c}{4\pi f_1})^2 (\max(D, r_o))^{-\eta}$, problem (16) is equivalently transformed as

$$\begin{aligned} & \max_{f_1} \hat{F}(f_1) \\ & \text{s.t. } \tilde{\text{C3}}, \end{aligned} \quad (\text{A.1})$$

where

$$\hat{F}(f_1) = f_1^{-2} \left(L - \frac{L^3 \pi^2 f_1^2}{6c^2} \left(1 - \frac{f_{\text{co}}^2}{2f_1^2} - \cos \theta \right)^2 \right). \quad (\text{A.2})$$

Taking the first-order and second-order derivatives of $\hat{F}(f_1)$ with respect to f_1 yields

$$\frac{\partial \hat{F}}{\partial f_1} = -2f_1^{-3} \left(L + \frac{L^3 \pi^2 f_{\text{co}}^2}{6c^2} \left(1 - \frac{f_{\text{co}}^2}{2f_1^2} - \cos \theta \right) \right), \quad (\text{A.3})$$

and

$$\frac{\partial^2 \hat{F}}{\partial f_1^2} = 6f_1^{-4} \left(L + \frac{L^3 \pi^2 f_{\text{co}}^2}{6c^2} (1 - \cos \theta) \right) - 5f_1^{-6} \frac{L^3 \pi^2 f_{\text{co}}^4}{6c^2}, \quad (\text{A.4})$$

respectively. Then, the solutions of $\frac{\partial \hat{F}}{\partial f_1} = 0$ and $\frac{\partial^2 \hat{F}}{\partial f_1^2} = 0$ are given by

$$f_1^{(1)} = \frac{f_{\text{co}}^2}{\sqrt{\frac{12c^2}{L^2 \pi^2} + 2(1 - \cos \theta) f_{\text{co}}^2}}, \quad (\text{A.5})$$

and

$$f_1^{(2)} = \frac{\sqrt{5} f_{\text{co}}^2}{\sqrt{\frac{36c^2}{L^2 \pi^2} + 6(1 - \cos \theta) f_{\text{co}}^2}}, \quad (\text{A.6})$$

respectively. According to (A.4) and (A.6), we see that $\frac{\partial^2 \hat{F}}{\partial f_1^2} < 0$ as $f_1 \in (0, f_1^{(2)})$, and $\frac{\partial^2 \hat{F}}{\partial f_1^2} > 0$ as $f_1 \in (f_1^{(2)}, \infty)$. Since $f_1^{(1)} < f_1^{(2)}$, we have $\frac{\partial \hat{F}}{\partial f_1} > \frac{\partial \hat{F}}{\partial f_1} \big|_{f_1=f_1^{(1)}} = 0$ as $f_1 \in (0, f_1^{(1)})$, and $\frac{\partial \hat{F}}{\partial f_1} < 0$ as $f_1 \in (f_1^{(1)}, \infty)$. Therefore, $f_1^{(1)}$ is the optimal solution for maximizing the objective function of problem (A.1). Considering (A.5) and the constraint C3, we obtain **Theorem 1**.

APPENDIX B: PROOF OF THEOREM 2

As mentioned in Appendix A and **Theorem 1**, frequencies are selected to maximize the $\hat{F}(f)$ given by (A.2), and $\hat{F}(f)$ is the increasing function of f as $f \in (0, f_1^*)$, and the decreasing function of f as $f \in (f_1^*, \infty)$. Let $f_{\min} = \min \{f_1^*, \dots, f_{n-1}^*\}$, if the center frequency f_n of the n -th satisfies $f_n \in (0, f_1^*)$, it should meet the following condition

$$f_n + \frac{B_n}{2} = f_{\min} - \frac{B_{\min}}{2}, \quad (\text{B.1})$$

where B_{\min} is the bandwidth of the subchannel with the center frequency f_{\min} . Based on the problem (16), we see that $B_n = 2f_n \frac{10^{\varepsilon/20} - 1}{10^{\varepsilon/20} + 1}$, and $B_{\min} = 2f_{\min} \frac{10^{\varepsilon/20} - 1}{10^{\varepsilon/20} + 1}$. Thus, (B.1) is rewritten as

$$f_n = 10^{-\varepsilon/20} f_{\min}. \quad (\text{B.2})$$

Likewise, let $f_{\max} = \max \{f_1^*, \dots, f_{n-1}^*\}$, if the center frequency f_n of the n -th satisfies $f_n \in (f_1^*, \infty)$, we have

$$f_n = 10^{\varepsilon/20} f_{\max}. \quad (\text{B.3})$$

Based on (A.1), (B.2) and (B.3), we find that the optimal f_n is $10^{-\varepsilon/20} f_{\min}$ when $\hat{F}(10^{-\varepsilon/20} f_{\min}) > \hat{F}(10^{\varepsilon/20} f_{\max})$, otherwise it is $10^{\varepsilon/20} f_{\max}$. As such, we obtain **Theorem 2**.

APPENDIX C: PROOF OF THEOREM 3

Let $F_{\text{EE}}(q_n) = \frac{1}{\ln 2} \frac{\ln(1+q_n \Xi_n)}{q_n + q_c}$, which is the objective function of problem (23). Taking the first-order derivative of F_{EE} yields

$$\frac{\partial F_{\text{EE}}}{\partial q_n} = \frac{1}{\ln 2} \frac{\hat{F}_{\text{EE}}(q_n)}{(q_n + q_c)^2}, \quad (\text{C.1})$$

where

$$\hat{F}_{\text{EE}}(q_n) = \frac{q_n + q_c}{1 + q_n \Xi_n} \Xi_n - \ln(1 + q_n \Xi_n). \quad (\text{C.2})$$

Since $\frac{\partial \hat{F}_{\text{EE}}}{\partial q_n} = -\frac{(q_c + q_n) \Xi_n^2}{(1 + q_n \Xi_n)^2} < 0$, $\hat{F}_{\text{EE}}(q_n)$ is a decreasing function of q_n . Based on the constraints $\hat{\text{C1}}$ and $\hat{\text{C2}}$, we see that $\frac{\gamma_{\text{th}}}{\Xi_n} < q_n < q_{\max}$. Then, two cases need to be considered as follows:

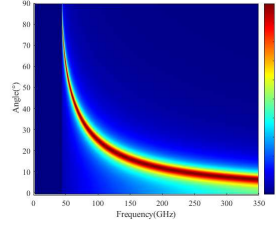
- Case 1: When $\hat{F}_{\text{EE}}(q_{\max}) \geq 0$, $\hat{F}_{\text{EE}}(q_n) > 0$ and thus $\frac{\partial F_{\text{EE}}}{\partial q_n} > 0$ for $q_n \in \left(\frac{\gamma_{\text{th}}}{\Xi_n}, q_{\max}\right]$, i.e., $F_{\text{EE}}(q_n)$ is an increasing function of q_n , hence the optimal q_n^* is $q_n^* = q_{\max}$.
- Case 2: When $\hat{F}_{\text{EE}}(q_{\max}) < 0$, q_o with $\hat{F}_{\text{EE}}(q_o) = 0$ can be easily obtained by using a one-dimension search for $q_o \in (0, q_{\max}]$. Then, we see that $\frac{\partial F_{\text{EE}}}{\partial q_n} \geq 0$ for $q_n \in (0, q_o]$ and $\frac{\partial F_{\text{EE}}}{\partial q_n} < 0$ for $q_n \in (q_o, q_{\max}]$. Therefore, $q_n^* = \max \left\{ q_o, \frac{\gamma_{\text{th}}}{\Xi_n} \right\}$ is the optimal solution.

As such, we get the optimal q_n^* given in **Theorem 3**.

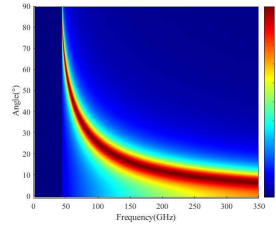
REFERENCES

- [1] 3GPP TS 38.104 v16.4.0, “NR; Base Station (BS) radio transmission and reception (Release 16),” June 2020.
- [2] S. Koenig *et al.*, “Wireless sub-THz communication system with high data rate,” *Nature Photonics*, vol. 7, pp. 977–981, Dec. 2013.
- [3] T. S. Rappaport *et al.*, “Wireless communications and applications above 100 GHz: Opportunities and challenges for 6G and beyond,” *IEEE Access*, vol. 7, pp. 78 729–78 757, June 2019.
- [4] K. Rikkinen, P. Kyöti, M. E. Leinonen, M. Berg, and A. Pärssinen, “THz radio communication: Link budget analysis toward 6G,” *IEEE Commun. Mag.*, vol. 58, no. 11, pp. 22–27, Nov. 2020.
- [5] S. Sun, T. S. Rappaport, R. W. Heath, Jr., A. Nix, and S. Rangan, “MIMO for millimeter-wave wireless communications: Beamforming, spatial multiplexing, or both?” *IEEE Commun. Mag.*, vol. 7, no. 12, pp. 110–121, Dec. 2014.
- [6] O. E. Ayach, S. Rajagopal, S. Abu-Surra, Z. Pi, and R. W. Heath, Jr., “Spatially sparse precoding in millimeter wave MIMO systems,” *IEEE Trans. Wireless Commun.*, vol. 13, no. 3, pp. 1499–1513, Mar. 2014.
- [7] C. Lin and G. Y. Li, “Energy-efficient design of indoor mmWave and Sub-THz systems with antenna arrays,” *IEEE Trans. Wireless Commun.*, vol. 15, no. 7, pp. 4660–4672, July 2016.
- [8] Z. Chen, X. Ma, B. Zhang, Y. Zhang, Z. Niu, N. Kuang, W. Chen, L. Li, and S. Li, “A survey on terahertz communications,” *China Commun.*, vol. 16, no. 2, pp. 1–35, Feb. 2019.
- [9] B. Peng, S. Wesemann, K. Guan, W. Templ, and T. Kürner, “Precoding and detection for broadband single carrier terahertz massive MIMO systems using LSQR algorithm,” *IEEE Trans. Wireless Commun.*, vol. 18, no. 2, pp. 1026–1040, Feb. 2019.
- [10] L. You, X. Chen, X. Song, F. Jiang, W. Wang, X. Gao, and G. Fettweis, “Network massive MIMO transmission over millimeter-wave and terahertz bands: Mobility enhancement and blockage mitigation,” *IEEE J. Sel. Areas Commun.*, vol. 38, no. 12, pp. 2946–2960, Dec. 2020.
- [11] L. Yan, C. Han, and J. Yuan, “A dynamic array-of-subarrays architecture and hybrid precoding algorithms for terahertz wireless communications,” *IEEE J. Sel. Areas Commun.*, vol. 38, no. 9, pp. 2041–2056, Sept. 2020.
- [12] X. Fu, F. Yang, C. Liu, X. Wu, and T. J. Cui, “Terahertz beam steering technologies: From phased arrays to field-programmable metasurfaces,” *Adv. Opt. Mater.*, vol. 8, no. 3, pp. 1–22, Feb. 2020.
- [13] G. Zhang, Q. Zhang, Y. Chen, T. Guo, C. Caloz, and R. D. Murch, “Dispersive feeding network for arbitrary frequency beam scanning in array antennas,” *IEEE Trans. Antennas Propag.*, vol. 65, no. 6, pp. 3033–3040, June 2017.
- [14] Y. Ghasempour, C. Yeh, R. Shrestha, D. Mittleman, and E. Knightly, “Single shot single antenna path discovery in THz networks,” in *Proc. 26th MobiCom*, 2020, pp. 1–13.
- [15] A. A. Oliner and D. R. Jackson, “Leaky-wave antennas,” in *Antenna Engineering Handbook*, J. L. Volakis, Ed. New York: McGraw-Hill, 2007.
- [16] D. R. Jackson and A. A. Oliner, “Leaky-wave antennas,” in *Modern Antenna Handbook*, C. Balanis, Ed. New York: Wiley, 2008.
- [17] D. R. Jackson, C. Caloz, and T. Itoh, “Leaky-wave antennas,” *Proc. IEEE*, vol. 100, no. 7, pp. 2194–2206, July 2012.
- [18] I. Bahl and K. Gupta, “Frequency scanning by leaky-wave antennas using artificial dielectrics,” *IEEE Trans. Antennas Propag.*, vol. 23, no. 4, pp. 584–589, July 1975.
- [19] G. Zhang, Q. Zhang, S. Ge, Y. Chen, and R. D. Murch, “High scanning-rate leaky-wave antenna using complementary microstrip-slot stubs,” *IEEE Trans. Antennas Propag.*, vol. 67, no. 5, pp. 2913–2922, May 2019.
- [20] N. J. Karl, R. W. McKinney, Y. Monnai, R. Mendis, and D. M. Mittleman, “Frequency-division multiplexing in the terahertz range using a leaky-wave antenna,” *Nature Photonics*, vol. 9, pp. 717–721, Sept. 2015.

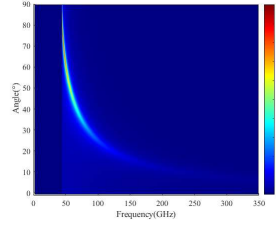
- [21] K. Murano, I. Watanabe, A. Kasamatsu, S. Suzuki, M. Asada, W. Withayachumnankul, T. Tanaka, and Y. Monnai, "Low-profile terahertz radar based on broadband leaky-wave beam steering," *IEEE Trans. Terahertz Sci. Technol.*, vol. 7, no. 1, pp. 60–69, Jan. 2017.
- [22] Y. Amarasinghe, R. Mendis, and D. M. Mittleman, "Real-time object tracking using a leaky THz waveguide," *Opt. Express*, vol. 28, no. 12, pp. 17 997–18 005, June 2020.
- [23] H. Matsumoto, I. Watanabe, A. Kasamatsu, and Y. Monnai, "Integrated terahertz radar based on leaky-wave coherence tomography," *Nature Electronics*, vol. 3, pp. 122–129, Feb. 2020.
- [24] C.-Y. Yeh, Y. Ghasempour, Y. Amarasinghe, D. M. Mittleman, and E. W. Knightly, "Security in terahertz WLANs with leaky wave antennas," in *ACM WiSec*, 2020, pp. 1–11.
- [25] T. S. Rappaport, G. R. MacCartney, Jr., M. K. Samimi, and S. Sun, "Wideband millimeter-wave propagation measurements and channel models for future wireless communication system design," *IEEE Trans. Commun.*, vol. 63, no. 9, pp. 3029–3056, Sept. 2015.
- [26] M. Haenggi, J. G. Andrews, F. Baccelli, O. Dousse, and M. Franceschetti, "Stochastic geometry and random graphs for the analysis and design of wireless networks," *IEEE J. Sel. Areas Commun.*, vol. 27, no. 7, pp. 1029–1046, Sept. 2009.
- [27] A. Sutinjo, M. Okoniewski, and R. H. Johnston, "Radiation from fast and slow traveling waves," *IEEE Antennas Propag. Mag.*, vol. 50, no. 4, pp. 175–181, Aug. 2008.
- [28] R. Mendis and D. M. Mittleman, "A 2-D artificial dielectric with $0 \leq n < 1$ for the terahertz region," *IEEE Trans. Microw. Theory Techn.*, vol. 58, no. 7, pp. 1993–1998, July 2010.
- [29] J. G. Andrews, T. Bai, M. N. Kulkarni, A. Alkhateeb, A. K. Gupta, and R. W. Heath, Jr., "Modeling and analyzing millimeter wave cellular systems," *IEEE Trans. Commun.*, vol. 65, no. 1, pp. 403–430, Jan. 2017.
- [30] M. K. Samimi *et al.*, "28 GHz angle of arrival and angle of departure analysis for outdoor cellular communications using steerable beam antennas in New York City," in *Proc. IEEE VTC*, Jun. 2013, pp. 1–6.
- [31] K. A. Hamdi, "Capacity of MRC on correlated Rician fading channels," *IEEE Trans. Commun.*, vol. 56, no. 5, pp. 708–711, May 2008.
- [32] Y. Zhu, L. Wang, K.-K. Wong, and R. W. Heath, Jr., "Secure communications in millimeter wave ad hoc networks," *IEEE Trans. Wireless Commun.*, vol. 16, no. 5, pp. 3205–3217, May 2017.
- [33] S. H. Han and J. H. Lee, "An overview of peak-to-average power ratio reduction techniques for multicarrier transmission," *IEEE Wireless Commun.*, vol. 12, no. 2, pp. 56–65, Apr. 2005.
- [34] G. Yu, S. He, D. Yu, L. Yang, , and G. Zuo, "An efficient low PAPR training sequence design scheme under spectral constraints in mm-Wave OFDM communication," in *Int. Conf. Wireless Commun. Signal Process. (WCSP)*, 2015, pp. 1–5.
- [35] S. Shakib, M. Elkholy, J. Dunworth, V. Aparin, and K. Entesari, "A wideband 28GHz power amplifier supporting 8×100MHz carrier aggregation for 5G in 40nm CMOS," in *IEEE Int. Solid-state Circuits Conf. (ISSCC)*, 2017, pp. 44–46.
- [36] F. Wang, T.-W. Li, and H. Wang, "A highly linear super-resolution mixed-signal doherty power amplifier for high-efficiency mm-Wave 5G Multi-Gb/s communications," in *IEEE Int. Solid-state Circuits Conf. (ISSCC)*, 2019, pp. 88–90.
- [37] J. Kokkonen, J. Lehtomäki, and M. Juntti, "Simple molecular absorption loss model for 200-450 gigahertz frequency band," in *Proc. European Conf. Netw. Commun. (EuCNC)*, 2019, pp. 219–223.
- [38] J. Kokkonen, J. Lehtomäki, and M. Juntti, "A line-of-sight channel model for the 100-450 gigahertz frequency band," *arXiv preprint arXiv:2002.04918*, pp. 1–14, Feb. 2020.
- [39] 3GPP TR 36.814, "Further Advancements for E-UTRA Physical Layer Aspects (Release 9)," Mar. 2010.
- [40] S. H. A. Shah, S. Aditya, S. Dutta, C. Slezak, and S. Rangan, "Power efficient discontinuous reception in THz and mmWave wireless systems," in *IEEE SPAWC*, 2019, pp. 1–5.



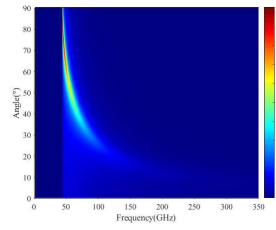
(a) Radiation pattern,
 $\alpha = 30\text{rad/m}$



(b) Radiation pattern, $\alpha = 60\text{rad/m}$



(c) Receive SNR with $\alpha = 30\text{rad/m}$



(d) Receive SNR with $\alpha = 60\text{rad/m}$

Fig. 3. Angle-frequency coupling behaviors for leaky-wave antenna in terms of the normalized radiation pattern and receive signal-to-noise ratio (SNR), where $L = 5.5\text{cm}$, $d = 3.5\text{mm}$, $q_t = -71.76\text{dBm/Hz}$, $\sigma_o^2 = -168\text{dBm/Hz}$, the free-space path loss model is adopted with a fixed distance $r_o = 50\text{m}$ [37, 38].

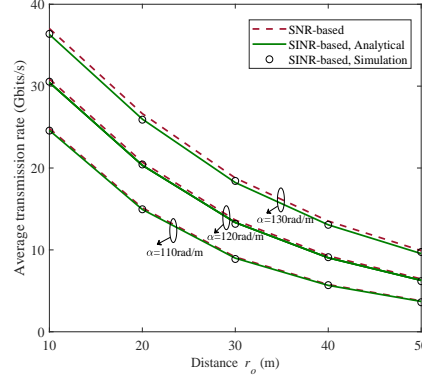


Fig. 4. The average transmission rate versus communication distance r_o for different α with $\lambda_{\text{THz}} = 5 * 10^{-1}/\text{m}^2$, $L = 0.06\text{m}$, $B_o = 5\text{GHz}$ and $f_o = 270\text{GHz}$ (namely the LoS direction of the typical receiver is $\theta_o = 28.7^\circ$ based on (2)).

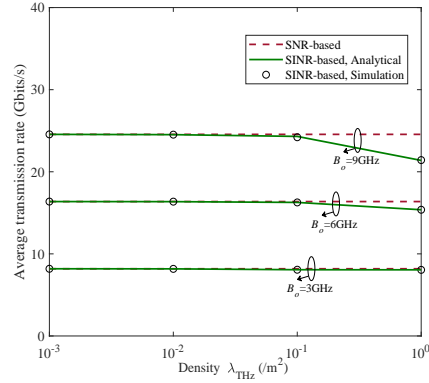


Fig. 5. The average transmission rate versus density λ_{THz} for different subchannel bandwidth B_o with $r_o = 30\text{m}$, $L = 0.06\text{m}$, $\alpha = 120\text{rad/m}$ and $f_o = 270\text{GHz}$ (namely $\theta_o = 28.7^\circ$).

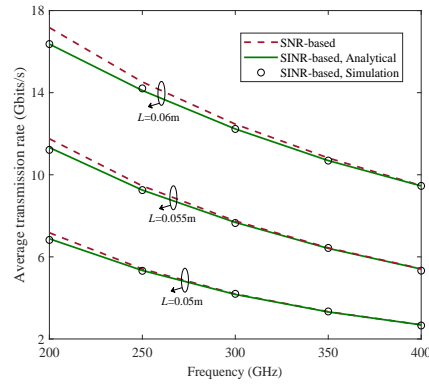
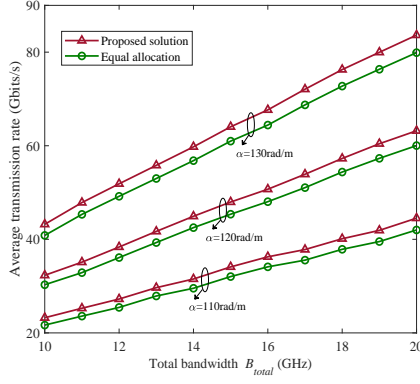
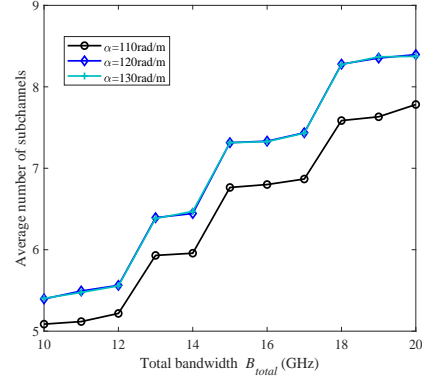


Fig. 6. The average transmission rate versus frequency for different L with $r_o = 30\text{m}$, $\lambda_{\text{THz}} = 5 * 10^{-1}/\text{m}^2$, $\alpha = 120\text{rad/m}$ and $B_o = 5\text{GHz}$.

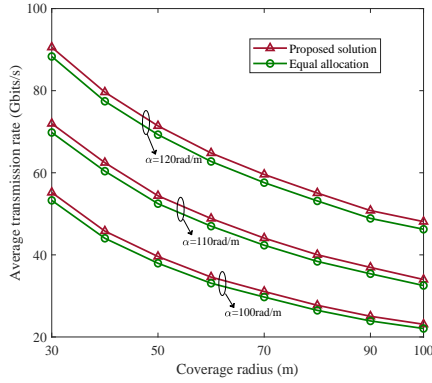


(a) Average transmission rate

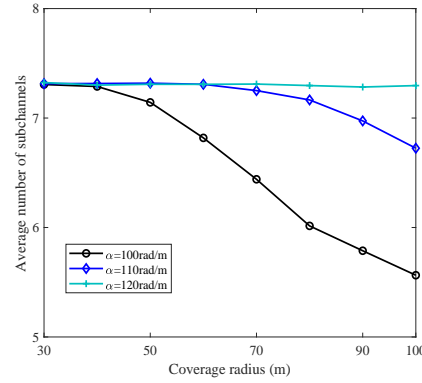


(b) Average number of subchannels

Fig. 7. The average transmission rate and number of subchannels versus total bandwidth for different α with the coverage radius $r_{\max} = 100\text{m}$.

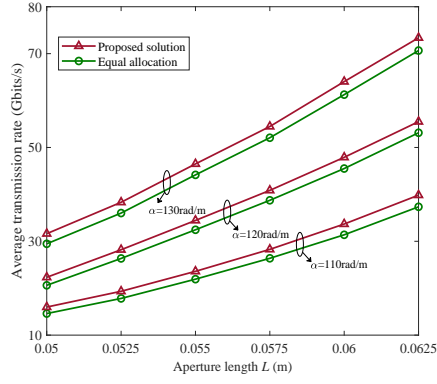


(a) Average transmission rate

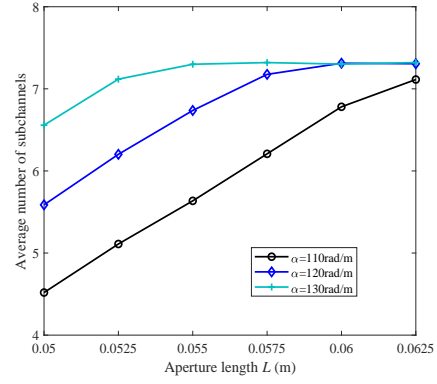


(b) Average number of subchannels

Fig. 8. The average transmission rate and number of subchannels versus coverage radius for different α with the total bandwidth $B_{total} = 15\text{GHz}$.

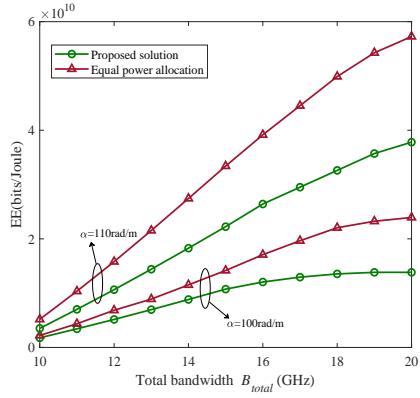


(a) Average transmission rate

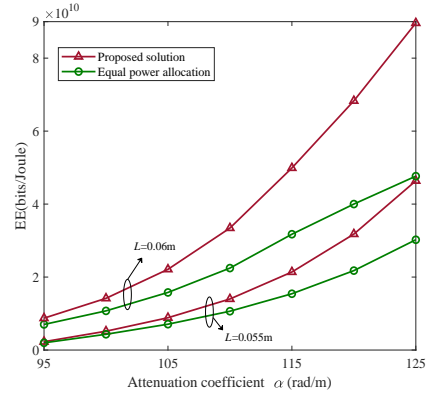


(b) Average number of subchannels

Fig. 9. The average transmission rate and number of subchannels versus aperture length for different α with the coverage radius $r_{\max} = 100\text{m}$ and the total bandwidth $B_{\text{total}} = 15\text{GHz}$.



(a) The EE versus total bandwidth for different α with the aperture length $L = 0.06\text{m}$.



(b) The EE versus attenuation coefficient for different L with the total bandwidth $B_{\text{total}} = 15\text{GHz}$.

Fig. 10. Energy efficiency (EE) enhancement.